Earthquake Research Advances 5 (2025) 100396

Contents lists available at ScienceDirect

Earthquake Research Advances

journal homepage: www.keaipublishing.com/en/journals/earthquake-research-advances

Rapid report of the March 28, 2025 M_W 7.9 Myanmar earthquake

Jing Cai*, Nan Xi, Guangjie Han, Wenze Deng, Li Sun

Early Warning and Quick Report Department, China Earthquake Networks Center, Beijing 100045, China

ARTICLE INFO

Keywords:
Focal mechanism
Rupture process
Real-time intensity

ABSTRACT

On March 28, 2025, a moment magnitude (M_W) 7.9 earthquake struck Myanmar, marking it as the most powerful seismic event of the year. The earthquake occurred along the Sagaing Fault, a prominent right-lateral strike-slip fault and the most significant active tectonic structure in Myanmar. In response to this seismic emergency, China Earthquake Networks Center (CENC) promptly published several reports on seismic source parameters. The focal mechanism solution indicates strike-slip faulting as the causative mechanism of the earthquake. Analysis of the rupture process indicates that it predominantly propagates from north to south. The rupture extended over a length exceeding 200 km and persisted for approximately 95 s. According to the estimated seismic intensity map, the meizoseismal region experienced shaking intensity reaching up to X(10), while the area with an intensity of more than VI exceeds 443 487 km^2. This earthquake inflicted substantial casualties and extensive property damage, underscoring the long-standing seismic hazard posed by the Sagaing Fault and highlighting the need for enhanced seismic preparedness and risk mitigation strategies in the region.

1. Introduction

At 14:20 Beijing time (12:50 local time in Myanmar) on March 28, 2025, a M_W 7.9 earthquake struck Myanmar. Given its significant magnitude, this seismic event inflicted extensive damage across Myanmar. Moreover, it had far-reaching impacts on neighboring regions, including Yunnan Province in China and Thailand, resulting in considerable losses. Statistically, the 2025 Myanmar earthquake represents the most powerful continental seismic event globally in the past decade and the strongest tremor to hit Myanmar in over a century. According to the authoritative report by the China Earthquake Networks Center (CENC), the hypocenter was located at 21.85°N and 95.95°E, with a focal depth of 30 km. Geographically, the epicenter was located 282 km from China's national border, near multiple administrative centers in Yunnan Province, China, such as Ruili City (310 km), Longchuan County (321 km), and Zhenkang County (364 km), and 776 km from Kunming City. Within a 300 km radius of the epicenter, 15 large and medium-sized cities were distributed. The terrain is located within a 5-km radius of the epicenter, having an average altitude of 69 m. The M_W 7.9 earthquake struck the densely populated city of Mandalay, where inadequate seismic design standards and poor lateral load-resistance capacities exacerbated structural collapses, leading to a significant surge in casualties. By 20:00 on April 4 (local time), this catastrophic earthquake had caused 3 354 fatalities, 4 508 injuries, and 220 people were still missing, along with inflicting varying degrees of damage on local housing and transportation infrastructure (https://www.163.com/dy/article/JSD4752B0534MHMX.html).

The M_W 7.9 earthquake in Myanmar occurred along the Sagaing Fault, a key tectonic boundary between the Indian and Sunda Plates. Trending north-south through Myanmar and extending into the Andaman Sea, this fault represents the largest and most active seismogenic threat in the country. Over extended periods, it has accumulated substantial tectonic stress from plate movements, historically generating over 10 earthquakes of M 7.0 or greater. Notably, the 1912 M_W 7.9 earthquake, which struck within a 300 km radius of the current

* Corresponding author.
E-mail addresses: caijing@seis.ac.cn (J. Cai), xinan314@seis.ac.cn (N. Xi), hangj@seis.ac.cn (G. Han), dengwenze@seis.ac.cn (W. Deng), sunli@seis.ac.cn (L. Sun).
Peer review under the responsibility of Editorial Board of Earthquake Research Advances.

Production and Hosting by Elsevier on behalf of KeAi

https://doi.org/10.1016/j.eqrea.2025.100396
Received 10 April 2025; Received in revised form 21 May 2025; Accepted 21 May 2025

epicenter, resulted in significant destruction, demonstrating the persistent seismic hazards associated with this fault zone.

To advance our understanding of the M_W 7.9 Myanmar earthquake and support emergency response efforts and future seismic hazard studies, we present a rapid earthquake report, similar to previous reports (Yang et al., 2022, 2024; An et al., 2023; Han et al., 2024), including tectonic setting and historical earthquake statistics, focal mechanism solutions, rupture propagation, estimated and instrumental intensity maps, etc.

2. Geological setting and historical earthquakes

Myanmar is located in the southeastern extension of the Mediterranean-Himalayan seismic belt and lies in the interaction zone of several geological blocks, including the Indian, Eurasian and Sunda plates, which have formed a number of active faults, including the right-slip Sagaing Fracture, on which the 7.9 magnitude earthquake in Myanmar occurred. The Sagaing Fault, which runs north-south through Myanmar and extends to the Andaman Sea, is the main active tectonic structure in Myanmar. It extends from the northern mountains of Myanmar to the Gulf of Mataban in the south, with a total length of about 1 400 km through the whole territory of Myanmar. It connects the discrete plate boundary in the Andaman Sea in the south with the continental collision zone of the Himalayan retrograde frontal margin in the north, and it is the key tectonic boundary between the Indian and Sunda plates (Kundu and Gahalaut, 2012; Tin et al., 2022; Zhu, 2022). The Sagaing Fault is the largest and most active source of seismic threat in Myanmar, traversing several core cities and densely populated areas, including Yangon, Naypyidaw, and Mandalay, and posing a significant disaster risk to millions of residents along its route.

As part of the eastern tectonic belt of the northward movement of the Indian Plate, the Sagaing Fault mainly absorbs the dextral strike-slip component generated during the oblique subduction of the plate. The Indian Plate is being squeezed by the Eurasian Plate towards the northeast at a rate of 4–5 cm per year, resulting in significant tectonic stress accumulation across the Sunda Plate boundary (Maurin et al., 2010; Aung et al., 2016). The Sagaing Fault endured prolonged compressive and shear stresses as a key segment of the plate boundary. Since 1900, at least 10 earthquakes with a magnitude exceeding 7.0 have occurred within a 300 km radius of the 2025 earthquake epicenter. Notable among these events is the 1912 earthquake (M_W 7.9), which struck near the 2025 epicenter, causing catastrophic damage. The 1946 earthquake (M_W 7.6), located 42 km north, resulted in thousands of casualties. The 2009 earthquake (M_W 7.5) further indicated ongoing

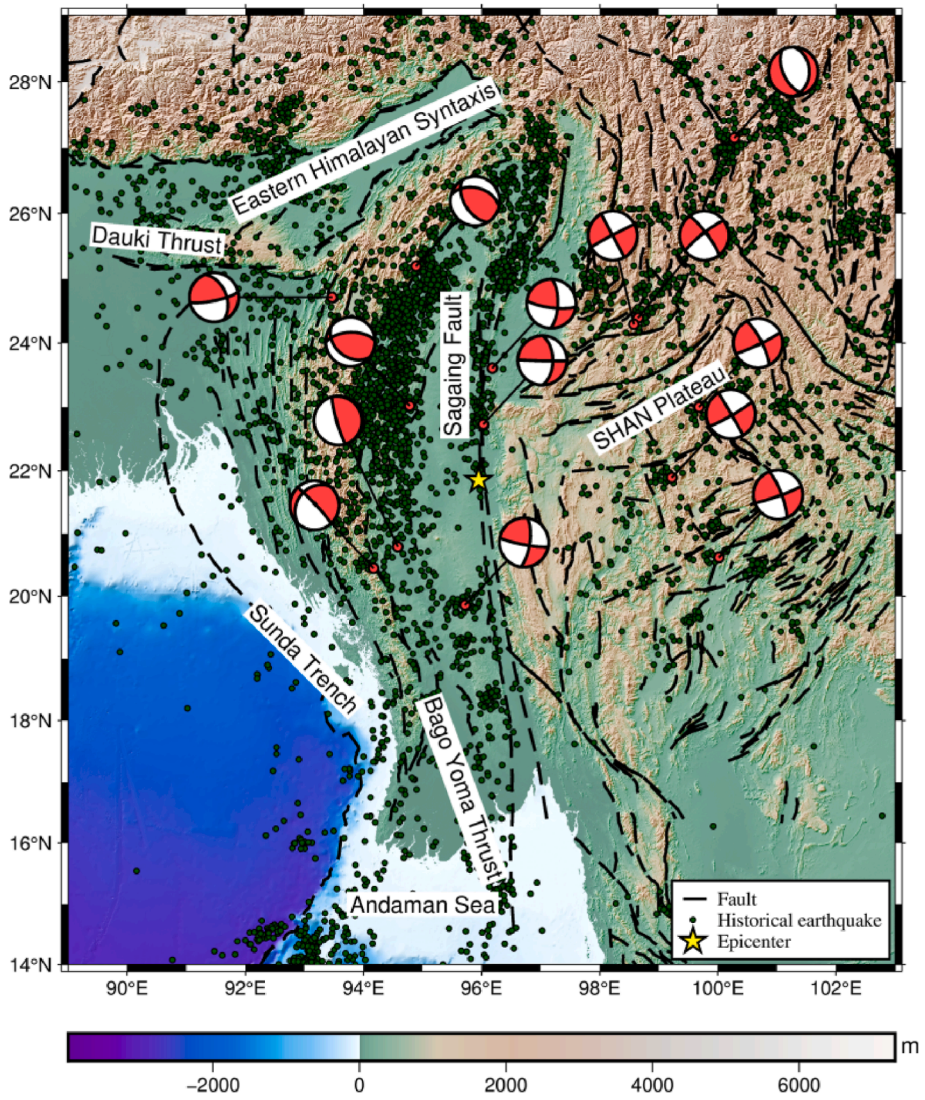

Fig. 1. Tectonic setting and historical earthquakes in the region. The yellow star represents the epicenter of the 2025 M_W 7.9 Myanmar Earthquake. Dark green circles indicate historical earthquakes ($M \geq 3.0$). Black lines represent the main faults. The red and white beachballs represent the focal mechanism ($M_W \geq 6.5$).

tectonic stress release in the region. Focal mechanism analyses of historical earthquakes near this area reveal predominant strike-slip and thrust faulting regimes (Fig. 1), consistent with the Sagaing Fault's dual role in accommodating both lateral shearing and compressional deformations.

3. Focal mechanisms

The seismic moment tensor provides information such as the physical processes of the earthquake source, scalar seismic moment, moment magnitude, fault type, and direction of movement. It reveals the nature of the seismogenic fault and its tectonic significance. The rapid determination of the moment tensor of a destructive earthquake is of great significance for earthquake disaster assessment, emergency rescue, research on the crustal stress field, and the simulation of strong ground motion. The WCMT method utilizes the characteristics of W-phase seismic waves, including a long period, relatively large group velocity, relatively simple waveforms, insensitivity to lateral crustal structure changes, and immunity from the amplitude limiting of records caused by S-waves or surface waves (Kanamori et al., 2008; Hayes et al., 2009). Using this method, the source depth, moment magnitude, strike, dip, and rake angles of the earthquake were determined. Upon receiving the official earthquake quick report information, our system automatically captured the event waveforms. Subsequently, these waveforms underwent a series of processing steps, including mean removal, Butterworth band-pass filtering, instrument response removal, effective waveform extraction, and rotation of the coordinate component. Finally, focal mechanism solutions were derived using the W-phase waveform inversion method (Duputel et al., 2013).

We derived the source depth, moment magnitude, strike, dip, and rake angles of the 2025 Myanmar earthquake. To verify the accuracy of the focal mechanism solutions obtained, we collected the results provided by several internationally authoritative institutions in the field of seismology. We used the Kagan angle (Kagan, 1991, 2005) to measure the differences between our solutions and these results. The Kagan angle is a key indicator for measuring the similarity or difference between the

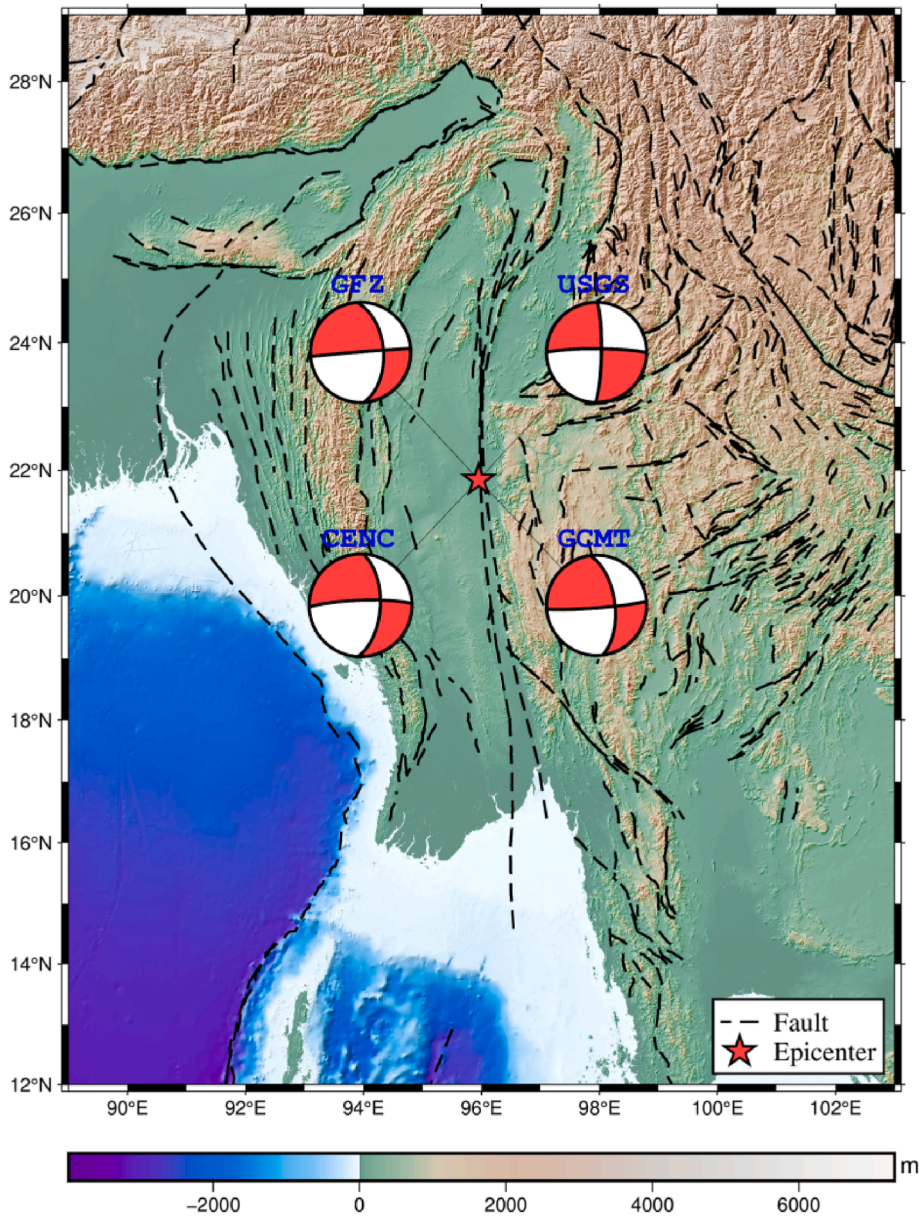

Fig. 2. Focal mechanism solutions of different agencies. The epicenter is marked by a red star, where black lines represent the main faults, and red and white beachballs represent the focal mechanism given by different seismological agencies.

two focal mechanism solutions. It comprehensively considers various parameters of the focal mechanism solutions, such as the strike, dip angle, and rake of the nodal planes, and then converts the differences in these parameters into a single angular value. This conversion makes a comparison between different focal mechanism solutions more intuitive and convenient. For example, if the Kagan angle between two focal mechanism solutions is 0°, it indicates that they are completely identical. Conversely, the larger the Kagan angle, the more significant the difference between the two focal mechanism solutions.

Fig. 2 presents the focal mechanisms of the 2025 Myanmar earthquake determined by different agencies. The strikes, dips, and rake angles of the two nodal planes provided by the China Earthquake Networks Center (CENC) are 268/82/-32 and 3/58/-170, respectively. The focal mechanism solution results from three institutions: the United States Geological Survey (USGS), the German Research Centre for Geosciences (GFZ), and the Global Centroid Moment Tensor (GCMT), are presented in Table 1. The Kagan angles between the focal mechanism solutions of these three institutions and that of the CENC are 22.79°, 9.85°, and 12.62°, respectively. Due to the influence of differences in seismic data, the selected methods, and the complexity of the velocity structure, the strike, dip, and rake angle show certain deviations among different earthquake agencies. The focal mechanism solution obtained by the CENC demonstrates a high degree of correspondence with those of the GFZ and GCMT. Furthermore, it is generally consistent with the results published by the USGS.

4. Rupture propagation

The rapid and accurate determination of the spatiotemporal characteristics of energy release during a major earthquake is crucial for precise disaster impact assessment and effective emergency response coordination. In this study, we employed two independent methodologies—backprojection of seismic waveforms and finite-fault kinematic inversion—to reconstruct the rupture process of the 2025 Myanmar earthquake.

4.1. The rupture process based on the back projection method

The Back-Projection Method is an important means for rapidly inverting the earthquake rupture process in seismology. It mainly images the spatiotemporal distribution of the rupture through the arrival time information of far-field seismic waves. Its core idea is to project the seismic waves backward from the observation points of the stations to the earthquake source region and locate the starting position and propagation process of the rupture through the focusing effect (Hara, 2007; Wang, 2017). Compared to the traditional finite-fault inversion method (Xu and Chen, 2022; Zhang et al., 2010), the array back projection method based on far-field P-wave data has significant advantages. This method does not involve source parameters, relies less on prior experience, eliminates complex steps such as the calculation of Green's functions, has a higher inversion efficiency, and the results are direct and highly stable (Wang et al., 2017; Chen et al., 2023).

We adopted the backprojection method based on far-field P-wave data to conduct an imaging analysis of the earthquake rupture process.

Table 1
Focal mechanism of the 2025 Myanmar earthquake from different international seismological agencies.

Nodal Plane I	Nodal Plane II	Depth (km)	M_W	Agency	Kagan angle relative to CENC (°)
Strike/Dip/ Rake angle (°)	Strike/Dip/ Rake angle (°)				
268/82/-32	3/58/-170	11	7.8	CENC	–
1/82/-174	270/84/-8	40.5	7.7	USGS	22.79
356/52/-179	266/89/-37	25	7.7	GFZ	9.85
353/60/175	85/86/30	19	7.7	GCMT	12.62

When selecting the network data for analysis, the main networks considered were those of China, Australia, and Europe. Among them, the Chinese network was not selected because the epicentral distance range was not appropriate, and it could not meet the requirements of this analysis. Although the European array can automatically acquire data in real-time, the amount of available data is limited, and the effect is not good when performing data stacking, making it difficult to achieve the desired analysis effect. The Australian seismic array, characterized by its dense station distribution and superior stacking resolution, yielded the primary rupture analysis results within the first hour post-earthquake.

To mitigate the influence of lateral heterogeneity in the subsurface structure on imaging location, the geometric center of the seismic array was adopted as a reference. The station closest to this center was selected as the reference station. Station correction values were obtained through cross-correlation calculations within the (0.05–1) Hz and (0.5–2) Hz frequency bands. During waveform stacking, only data with a correlation coefficient exceeding 0.6 were incorporated. This ensured the reliability of the stacking outcomes. A high-resolution model of the hypocentral region was developed by partitioning the hypocentral area into 5 km × 5 km equidistant grids at the hypocentral depth. In total, 149 × 149 grids were generated. Subsequently, the backprojection method was utilized to conduct stacking imaging on high-frequency data in the (0.5–2) Hz range. Analysis results indicate that the rupture strike of this earthquake is predominantly in the north-south (NS) direction. Calculations show that the earthquake rupture persisted for approximately 95 s, with a rupture length exceeding 200 km (Fig. 3).

4.2. The rupture process based on the finite-fault inversion method

We also employed the finite fault inversion method to conduct an inversion analysis of the source rupture process of the Myanmar earthquake. The finite fault inversion method typically treats the fault as a finite planar source with a specific length and width. It utilizes the wavelet domain to effectively separate signals in different frequency bands and applies the simulated annealing algorithm to solve for the spatiotemporal distribution pattern of the slip displacement on the fault plane (Ji et al., 2022a, 2022b).

During the data utilization and model construction stages, we collected far-field data with an epicentral distance ranging from 30° to 90°, which were obtained from the Global Seismographic Network (GSN) and the Federation of Digital Seismograph Networks (FDSN). The minimum signal-to-noise ratio of these data was 10. In the finite fault inversion, it is usually necessary to estimate the length and width of the fault. The estimation formulas for the length and width are, respectively, as follows (Dahlen et al., 1998),

$$L = V_r \times T_d \tag{1}$$

$$W = \frac{D}{\sin(\theta)} \times 2 \tag{2}$$

In Equa. (1), V_r represents the rupture velocity, and T_d represents the rupture duration. In Eq. (2), D presents the focal depth, and θ represents the dip angle of the fault plane.

Based on the interface parameters given by the focal mechanism solution (strike = 358°, dip = 75°, rake angle = −174°), a rupture plane model was constructed, and a plane with a length of 485 km and width of 26 km was selected as the rupture plane, which was divided into 275 subfaults (55 × 5). The epicenter position (21.85°N, 95.95°E) released by the China Earthquake Networks Center was taken as the initial rupture point. By integrating the research results of multiple international institutions, 10 km was set as the initial rupture depth.

In terms of waveform data screening, 27 sets of far-field P-wave and SH-wave waveform data were selected. These data not only have a relatively high signal-to-noise ratio but are also relatively evenly distributed along the azimuth angle. Through the rupture process

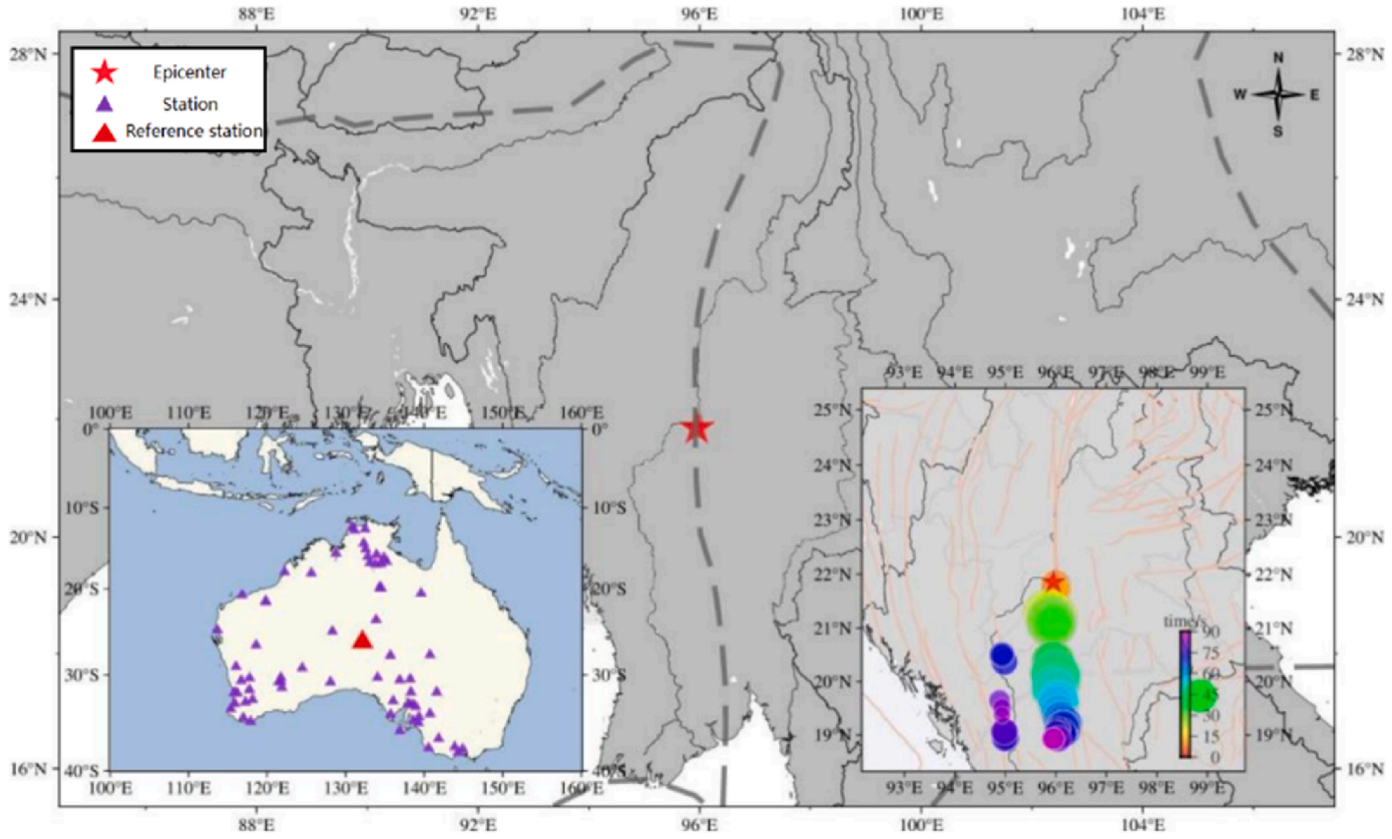

Fig. 3. The rupture process is obtained based on the back projection method. The red five-pointed star represents the epicenter, the red triangles represent the reference stations, and the purple triangles represent the stations.

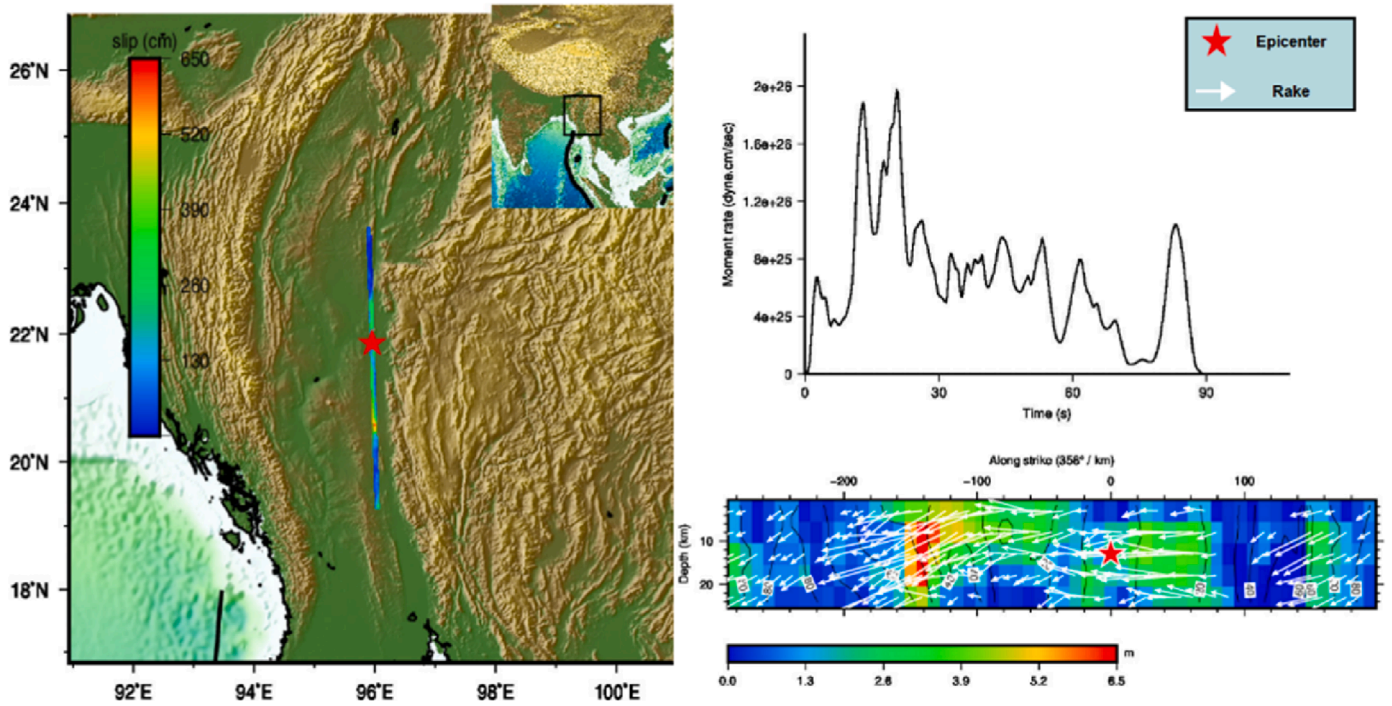

Fig. 4. The rupture process is determined using the finite-fault inversion method. The diagram on the upper right represents the source time function, and the diagram on the lower right represents the distribution of static slip displacement on the fault plane. The red five-pointed star represents the epicenter, and the white arrow represents the rake.

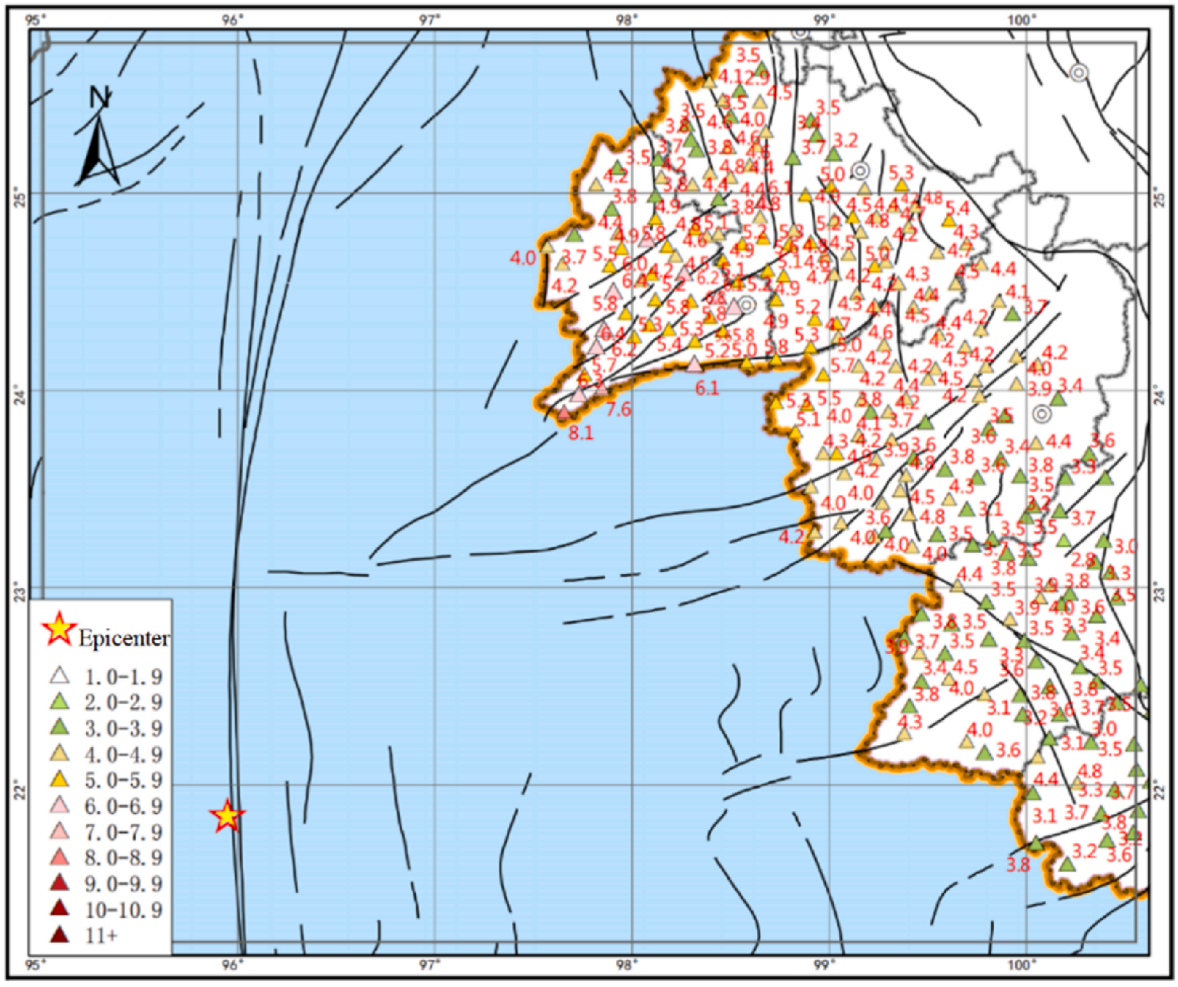

Fig. 5. Instrumental intensity map monitored within the territory of China. The yellow star represents the epicenter, and the black lines show the main faults.

inversion, we determined that the main rupture lasted approximately 90 s, extended over an area of approximately 260 km, and produced a maximum slip displacement of 6.5 m (Fig. 4).

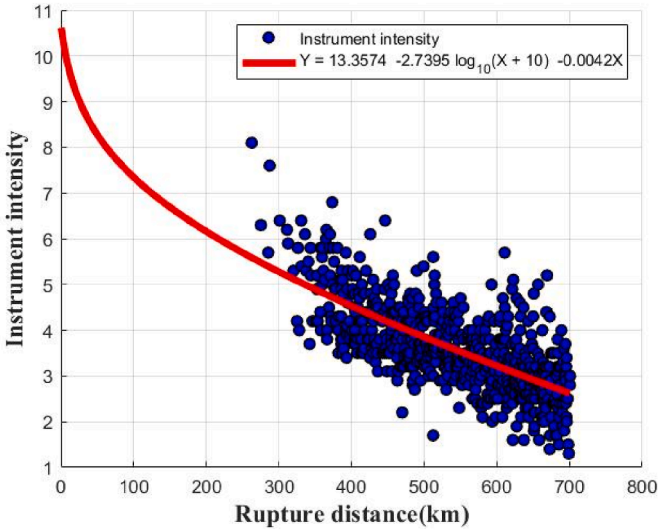

Fig. 6. The attenuation relationship between instrumental intensity and rupture distance.

The seismic rupture processes derived from the finite-fault inversion and back-projection method exhibit consistent overall trends, though slight discrepancies remain between them. This phenomenon can be attributed to two primary factors. First, the methods differ in data characteristics: the back-projection method employs high-frequency seismic data, whereas finite-fault inversion relies on low-frequency data. The fundamental divergence in their analysis frequency bands directly influences the result outputs. Second, inherent differences exist in their theoretical frameworks, including variations in physical assumptions and the logic of model construction. Collectively, the result disparities arising from these dual data- and methodological differences are regarded as normal phenomena in this context. Overall, the differences in results caused by the dual disparities in data characteristics and methodological theories are considered normal phenomena.

5. Instrumental intensity and estimated intensity

5.1. Instrumental intensity

Instrumental intensity, recorded by seismic monitoring instruments, directly reflects ground motion intensity at various locations during an earthquake, providing crucial data for assessing potential damage to buildings and infrastructure. We collected a total of 485 strong-motion stations within 700 km of the epicenter. According to the National Standard of the People's Republic of China (PRC), the Chinese Seismic Intensity Scale (GB/T 17742–2020), the recorded peak ground

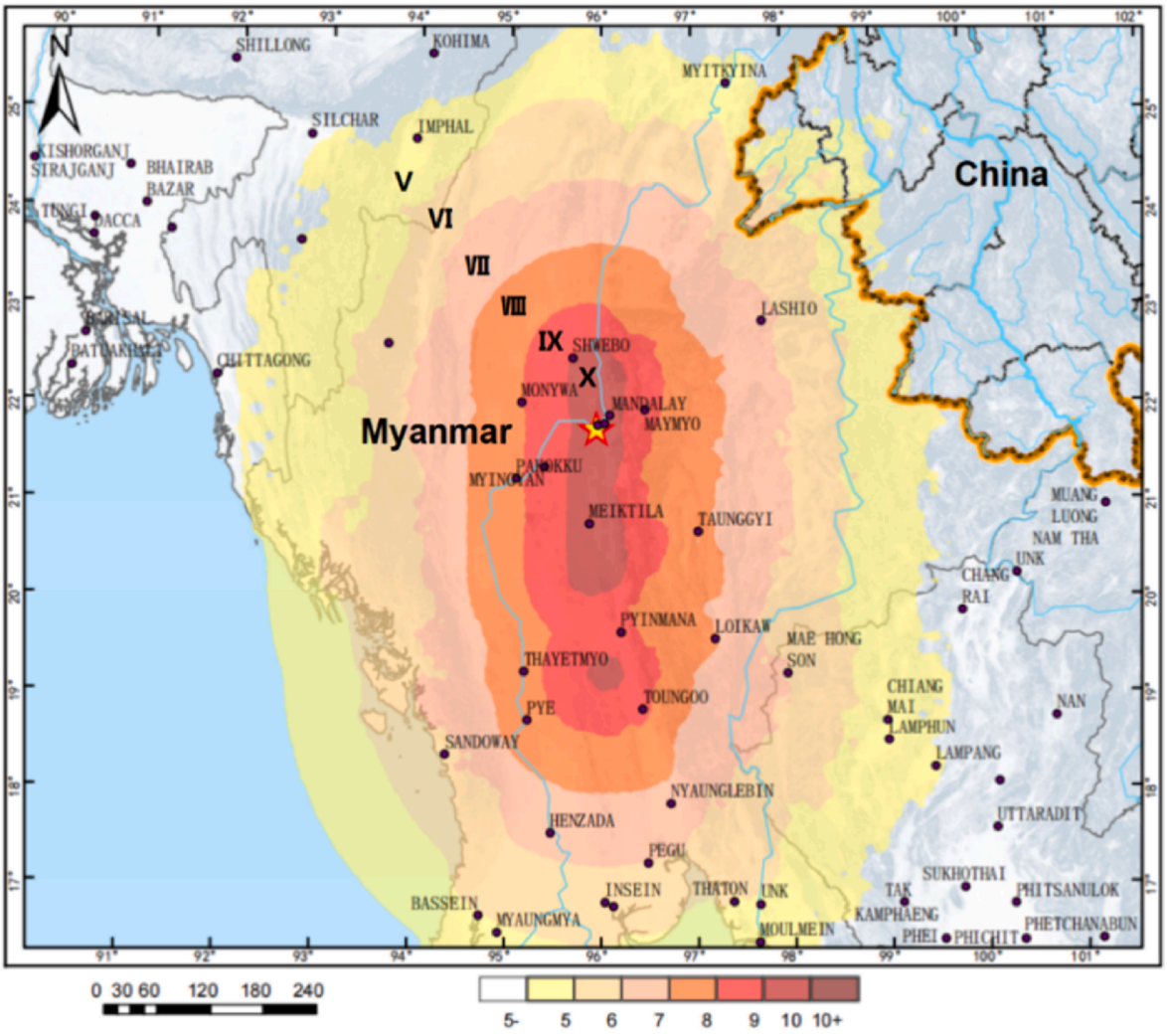

Fig. 7. Estimated intensity map of the M_W 7.9 Myanmar earthquake. The yellow star represents the epicenter. The Roman numerals V through X correspond to seismic intensity grades 5 to 10 in the Chinese intensity scale.

acceleration (PGA) and peak ground velocity (PGV) were converted to seismic intensity. Fig. 5 shows that the maximum instrument intensity is 8.1, with a peak ground acceleration of ~76.8 cm/s^2 and a peak ground velocity of about 22.9 cm/s. The location where this maximum intensity was recorded is near Nongdao Town, Ruili City, Dehong Dai and Jingpo Autonomous Prefecture, Yunnan Province, which is approximately 284.31 km away from the epicenter.

5.2. Estimated intensity

We estimated the intensity map of the Myanmar earthquake using continuous real-time data. Given the lack of strong motion observation data in Myanmar, we used strong motion data recorded by the Yunnan Seismic Network in China to calculate estimated seismic intensity. First, virtual stations are established to achieve a more uniform distribution of stations. Based on the extent of earthquake fault rupture, instrumental intensity value, and fault distance, we calculated the measured attenuation relationship (see Equa. (3)). Subsequently, this attenuation relationship is employed to estimate the intensity of each virtual station. Finally, the site correction was carried out using the slope-based global V_S30 model (Allen and Wald, 2007) to obtain the estimated intensity distribution of this earthquake. The site correction process entailed three sequential steps: (1) Derivation of V_S30 values from global 30-arcsecond topographic slope data using a slope-based global V_S^{30} model; (2) Categorization of site classes per the NEHRP system using the derived V_S30 values; (3) Calibration of PGA and PGV for each site class using site amplification factors (Borcherdt, 1994). Fig. 6 presents the scatter plot distribution of the instrumental intensity and rupture distance of this earthquake, along with the corresponding regression curve.

The calculation results indicate that the highest seismic intensity reached X degree, with the high-intensity zone distributed along the ruptured fault, spanning over 400 km from north to south. The area experiencing intensity VI(6) or higher covers approximately 443 487 square kilometers and has had a notable impact on India, Thailand, and China's Yunnan region. (Fig. 7).

$$Y = 13.3574 - 2.7395 \log_{10}(X + 10) - 0.0042X \pm 0.6855 \quad (3)$$

where Y represents the instrumental intensity, and X represents the fault distance, the unit is kilometers.

It should be noted that due to the limitations of seismic monitoring data in Myanmar, this study uses data from the Yunnan Seismic Network. However, regional tectonic differences along the China-Myanmar border, seismic wave propagation path effects, and other factors may introduce certain errors in the attenuation relationships. Future research may combine local strong-motion data with attenuation relationships to further correct the inferred intensity biases.

6. Discussion and conclusion

This paper presents a preliminary analysis of the M_W 7.9 earthquake that struck Myanmar in 2025. The earthquake occurred along the Sagaing Fault Zone. The focal mechanism solution reveals that this earthquake is associated with a strike-slip fault. Analysis of the rupture process shows that the rupture is predominantly oriented in a north-south (NS) direction, demonstrating unilateral southward rupture propagation. The largest intensity value recorded by the strong-motion stations reached 8.1 on the instrumental scale. This peak intensity was detected at station N0203, which is situated 284.31 km from the epicenter of the earthquake. The estimated intensity map shows a seismic intensity reaching up to X degree within the meizoseismal region, and the area with an intensity of VI degree or higher covers approximately 443 487 km^2. This earthquake exerted tremendous destructive force, inflicting severe casualties and substantial property damage in Myanmar. We posit the following potential contributing factors: (1) This earthquake reached a magnitude of 7.9, releasing enormous energy. With a focal depth of just 30 km, it was a shallow-focus earthquake, resulting in minimal attenuation of seismic energy at the surface. This caused intense ground shaking and significantly increased the destructive force on buildings. (2) Buildings in Myanmar generally have a low seismic resistance grade and cannot withstand the impacts of strong earthquakes. (3) The epicenter was near Mandalay's urban core, a densely populated area where high population density expanded the disaster's impact, concentrating casualties and property losses. The seismic parameters, like focal mechanism, rupture process, and estimated intensity from this research, can offer more precise data for seismic hazard assessment in these areas. Thus, relevant departments can formulate better emergency plans based on our analysis of this earthquake's damage, strengthening response capabilities and reducing losses.

CRediT authorship contribution statement

Jing Cai: Writing – original draft, Conceptualization. **Nan Xi:** Visualization. **Guangjie Han:** Formal analysis. **Wenze Deng:** Data curation. **Li Sun:** Writing – review & editing.

Author agreement and acknowledgement

On behalf of my co-authors, I would like to declare that the research described in this manuscript is original and has not been published previously. The work is also not under consideration for publication elsewhere, either in whole or in part. All authors listed have approved the enclosed manuscript. The authors thank the scientists from China Earthquake Network Center for sharing their results shortly after the earthquake. We would like to acknowledge the support of the China Earthquake Network Center Youth Science and Technology Fund (QNJJ:202320).

Declaration of competing interest

The authors declare that they have no known competing financial interests or personal relationships that could have appeared to influence the work reported in this paper.

References

Allen, T.I., Wald, D., 2007. Topographic-slope as a proxy for seismic site conditions (V_s 30) and amplification around the globe. Center for Integrated Data Analytics. Wisconsin Science Center.

An, Y., Wang, D., Ma, Q., et al., 2023. Preliminary report of the September 5, 2022, M_S 6.8 Luding earthquake, Sichuan, China. Earthq. Res. Adv 3 (1), 10084.

Aung, P.S., Satirapod, C., Andrei, C.O., 2016. Sagaing Fault slip and deformation in Myanmar observed by continuous GPS measurements. Geodesy Geodyn. (1), 8. English Edition.

Borcherdt, R.D., 1994. Estimates of site-dependent response spectra for design (methodology and justification). Earthq. Spectra 10, 617–617. https://doi.org/10.1193/1.1585791.

Chen, W., Rao, G., Kang, D., et al., 2023. Early report of the source characteristics, ground motions, and casualty estimates of the 2023 M_W 7.8 and 7.5 Turkey earthquakes. J. Earth Sci. 34 (2), 297–303.

Dahlen, F.A., Tromp, J., 1998. Theoretical Global Seismology. Princeton University Press, Princeton, p. 178.

Duputel, Z., Rivera, L., Kanamori, H., et al., 2013. W-phase fast source inversion for moderate to large earthquakes (1990-2010). Geophys. J. Int. 189 (2), 1125–1147.

Han, G.J., et al., 2024. Rapid report of the December 18, 2023, M_S 6.2 Jishishan earthquake, Gansu, China. Earthq. Res. Adv. 4 (2). https://doi.org/10.1016/j.Accra.2024.100287.

Hara, T., 2007. Magnitude determination using duration of high-frequency energy radiation and displacement amplitude: application to tsunami earthquakes. Earth Planets Space 59 (6), 561–565.

Hayes, G.P., Rivera, L., Kanamori, H., et al., 2009. Source inversion of the W-phase: real-time implementation and extension to low magnitudes. Seismol Res. Lett. 80 (5), 817–822.

Ji, C., Wald, D.J., Helmberger, D.V., 2022a. Source description of the 1999 hector mine, California, earthquake, Part I: wavelet domain inversion theory and resolution analysis. Bull. Seismol. Soc. Am. 92 (4), 1192–1207.

Ji, C., Wald, D.J., Helmberger, D.V., 2022b. Source description of the 1999 hector mine, California, earthquake, Part II: complexity of slip history. Bull. Seismol. Soc. Am. 92 (4), 1192–1207.

Kagan, Y.Y., 1991. 3-D rotation of double-couple earthquake sources. Geophys. J. Int. 106 (3), 709–716.

Kagan, Y.Y., 2005. Double-couple earthquake focal mechanism: random rotation and display. Geophys. J. Int. 163 (3), 1065–1072. https://doi.org/10.1111/j.1365-246X.2005.02781.x.

Kanamori, H., Rivera, L., 2008. Source inversion of W phase: speeding up seismic tsunami warning. Geophys. J. Int. 175 (1), 222–238.

Kundu, B., Gahalaut, V.K., 2012. Earthquake occurrence processes in the Indo-Burmese wedge and Sagaing fault region. Tectonophysics 524–525, 135–146.

Maurin, T., Masson, F., Rangin, C., et al., 2010. First GPS results in northern Myanmar: constant and localised slip rate along the Sagaing fault. Egu Gen. Assemb. 12, 4544.

Tin, T.Z.H., Nishimura, T., Hashimoto, M., Lindsey, E., Aung, L.T., Min, S.M., et al., 2022. Present-day crustal deformation and slip rate along the southern Sagaing fault in Myanmar by GNSS observation. J. Asian Earth Sci.

Wang, D., Kawakatsu, H., Zhuang, J., et al., 2017. Automated determination of the magnitude and source, length of large earthquakes using back projection and P wave amplitudes. Geophys. Res. Lett. 44 (11).

Xu, L.S., Chen, Y.T., 2022. Source time function and source rupture process. Seismol. Geomagn. Obs. Res. 23 (6), 8 (in Chinese).

Yang, H., Wang, D., Guo, R., et al., 2022. Rapid report of the 8 January 2022 M_S 6.9 Menyuan earthquake, Qinghai, China. Earthquake Research Advances 2 (1), 11.

Yang, Z.G., et al., 2024. Towards fast focal mechanism inversion of shallow crustal earthquakes in the Chinese mainland. Earthq. Res. Adv. 4 (2).

Zhang, Y., Chen, Y.T., Xu, L.S., 2010. Rupture process of the 6 April 2009, L'Aquila, Italy, M_w 6.3 Earthquake-A comparison between apparent source time function method and the direct waveform inversion method (in Chinese). Chin. J. Geophys. 53 (6), 1428–1439.

Zhu, Y., 2022. Study on the Sagaing Fault in Southern Myanmar and the Indian Subduction Slab Based on Seismicity and Focal Mechanism Solutions. University of Chinese Academy of Sciences, Beijing.